

**Nanoconfined synthesis of conjugated ladder polymers**

Journal:	<i>Polymer Chemistry</i>
Manuscript ID	PY-REV-06-2022-000809.R1
Article Type:	Review Article
Date Submitted by the Author:	06-Aug-2022
Complete List of Authors:	Kitao, Takashi; The University of Tokyo, Applied Chemistry; JST-PRESTO, Zhang, Xiyuan; The University of Tokyo, Advanced Materials Science Uemura, Takashi; The University of Tokyo, Applied Chemistry

## REVIEW

# Nanoconfined synthesis of conjugated ladder polymers

Takashi Kitao,<sup>a,b</sup> Xiyuan Zhang<sup>c</sup> and Takashi Uemura<sup>a\*</sup>

Received 00th January 20xx,  
Accepted 00th January 20xx

DOI: 10.1039/x0xx00000x

Conjugated ladder polymers (CLPs) are an attractive type of macromolecule consisting of periodically repeated fused aromatic rings. Their rigid and fully conjugated backbones endow CLPs with intriguing optical, electronic, and magnetic properties. Current challenges of facing CLP chemistry are difficulty in regulating their synthesis due to unfavorable side reactions (e. g. cross-linking and branching) and their low solubility. Template-confined synthesis is a viable strategy for controlling CLP structures at the atomic scale. In this review, we describe recent developments and future perspectives in the confined synthesis of CLPs utilizing templates, including metal surfaces and nanoporous materials. Access to CLPs with greater diversity will contribute to the ability to control their intrinsic properties, paving the way to their future applications in many fields.

## 1. Introduction

Ladder polymers are defined as multi-stranded polymers consisting of fused rings, where adjacent rings share two or more atoms. Possessing backbones of fused aromatic rings, conjugated ladder polymers (CLPs) are intrinsically free from the torsional rotation of bonds between the monomeric units, in contrast to the flexible or semirigid nature of single-stranded conjugated polymers (Fig. 1).<sup>1–5</sup> Owing to their highly extended  $\pi$ -conjugation systems, CLPs exhibit several fascinating optoelectronic properties, such as narrow band gaps, high carrier mobilities, and long exciton diffusion lengths.<sup>3, 6–13</sup> Hence, CLPs are prime targets for numerous applications in optoelectronic devices including organic photovoltaics, light-emitting diodes, and thin-film transistors,<sup>14–16</sup> continuously stimulating the creativity of chemists to develop synthetic methods for CLPs.<sup>3, 6, 17</sup>

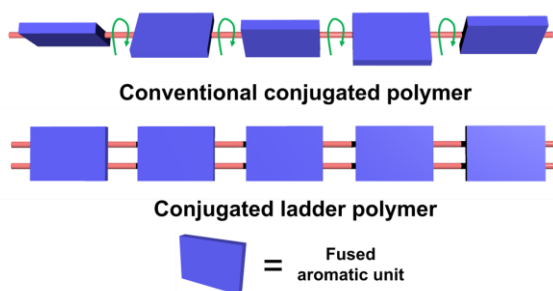


Fig. 1 Graphical representation of CLPs and conventional conjugated polymers connected by single bonds.

The synthetic strategies for CLPs can be divided into two distinct types. The first is single-step ladder formation, in which monomer units are connected by simultaneously forming multiple bonds, such as polycondensation of tetra-functional monomers or repetitive Diels–Alder cycloaddition.<sup>18–20</sup> The second approach involves the “zipping” of a pre-polymer, whereby a single-stranded polymer contains attached functional side moieties, including vinyl, sulfoxide, and aromatic C–H groups, that are then connected to form the ladder structure.<sup>21–27</sup> The development of synthetic methods has widened the scope of well-defined CLP syntheses. However, these synthesis strategies remain intrinsically challenging in solution because the formation of undesirable non-ladder defects, such as branching and cross-linking, cannot be avoided owing to the multiple reaction sites. Furthermore, strong interchain  $\pi$ - $\pi$  interactions render CLPs insoluble in common solvents, resulting in precipitation before the reactions are complete. Therefore, the monomer structures must be carefully designed to introduce solubilizing substituents that do not cause undesirable changes in the inherent physicochemical properties of CLPs.

Template-confined synthesis has recently emerged as a feasible and powerful approach for CLPs.<sup>6, 28–31</sup> Mediating the organization of the monomers/pre-polymers using templates (e. g. metal surfaces and nanoporous materials) allows for the regulation of reaction sites, providing CLPs that are otherwise inaccessible in solution. Confined propagation of the polymer chains can overcome solubility limitations by isolating individual chains. Moreover, this methodology provides control over the polymer assemblies, enabling the fabrication of nanostructured architectures that give rise to various unique optoelectronic properties. This review discusses recent developments in the confined synthesis of CLPs. We begin by introducing a diverse range of reaction fields amenable to CLP synthesis. We then

<sup>a</sup> Department of Applied Chemistry, Graduate School of Engineering, The University of Tokyo, 7-3-1 Hongo, Bunkyo-ku, Tokyo 113-8656, Japan. E-mail: uemurat@g.ecc.u-tokyo.ac.jp

<sup>b</sup> JST-PRESTO, Kawaguchi, Saitama 332-0012, Japan.

<sup>c</sup> Department of Advanced Materials Science, Graduate School of Frontier Sciences, The University of Tokyo, 5-1-5 Kashiwanoha, Kashiwa, Chiba 277-8561, Japan.

describe several attractive CLPs obtained in constrained media, and finally, detail viable future research directions in this field.

## 2. Reaction fields for synthesis of CLPs

### 2.1 Metal surfaces

The past decade has witnessed the significant development of on-surface synthesis with considerable potential for the bottom-up preparation of polymeric nanomaterials.<sup>32-37</sup> The surface can restrict intermolecular interactions to small dimensions, allowing for the rational synthesis of nanomaterials with diverse structures, ranging from one-dimensional (1D) polymer chains to two-dimensional (2D) networks. In this approach, the carefully designed organic building units are thermally sublimed and deposited on atomically clean metal surfaces, such as Au(111), Cu(111), Ag(111). Subsequent post annealing induce the polymerization of the monomers at predetermined (activated) sites. In general, surface reactions are conducted in an ultrahigh vacuum (UHV), allowing for a broader range of reaction temperatures without risk of air oxidation. In addition to the monomer design, the choice of metal surfaces is also a key step that dictates the polymerization outcome.<sup>38</sup> This is because the mobility and reactivity of the monomers are significantly affected by the metal surfaces, as seen in the case of Ullmann coupling of aryl halides on metal surfaces. Bieri et.al. performed polymerization of the hexaido-substituted macrocycle cyclohexa-*m*-phenylene (CHP) on metal surfaces.<sup>39</sup> The branched network structures dominated on Cu(111), whereas, the use of Ag(111) provided highly ordered and dense polyphenylene networks (Fig. 2). Monte Carlo simulations revealed that the CHP radical generated by thermal annealing on Ag(111) had a lower diffusion barrier than that of Cu(111), which means the radicals migrate over large distances to find appropriate positions, resulting in the formation of the ordered network structures.

The synthesis of CLPs on surfaces is characterized by several advantageous features. The polymerizations proceed directly on the surface without being hindered by the solubility issues that frequently occur in solution. The chemical structures of the final products and intermediates can be observed in detail using high-resolution analytical techniques, such as atomic force microscopy (AFM) and scanning tunneling microscopy (STM). Moreover, UHV conditions provide access to polymers that would be unstable under ambient conditions.

### 2.2 Nanospaces

Confined polymerizations in artificial nanospaces have been investigated over the past decades as a method for controlling the primary and two- and three-dimensional multi-level structures. Moreover, the shielding provided by the nanoconfinement can improve the stability of otherwise unstable intermediates and/or products even under ambient conditions.<sup>40-42</sup>

#### 2.2.1 Carbon nanotubes

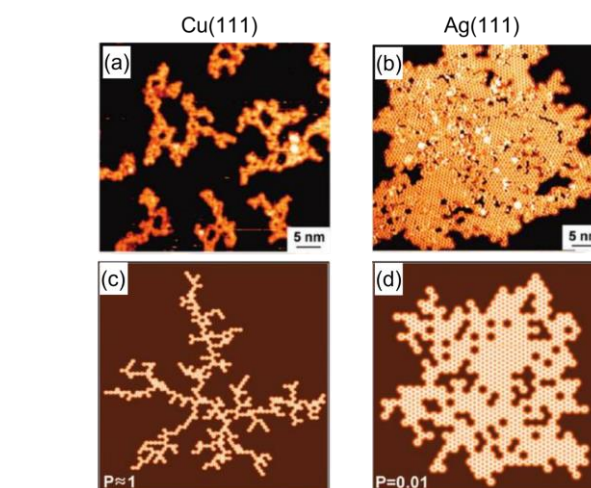


Fig. 2 Comparison of the formation of polymer networks from CHP precursor on metal surfaces. (a, b) STM images of (a) Cu(111) and (b) Ag(111). (c, d) Monte Carlo simulations with varying factor  $P$  corresponding to the ratio of the reactivity to the diffusivity of the CHP molecules. Reprinted with permission from ref. 39. Copyright 2010 American Chemical Society.

The interior space of carbon nanotubes (CNTs) is uniform, and their sizes are in the range of approximately 1 nm to several tens of nanometers. A variety of guest species can be encapsulated in CNTs, leading to preferential alignment of the monomers through the geometrical constraint; thus, the polymerization of the monomers within the CNTs induces the selective formation of quasi 1D nanomaterials.<sup>43-46</sup> Due to their high thermal and chemical stabilities, the polymerization reactions can be carried out even under harsh conditions, including hydrogen arc discharge and high thermal annealing, without risking damage to the host CNTs. These features highlight the potential of CNTs for a plethora of chemical reactions, affording various linear polymers, such as diamond nanowires and fullerene chains.<sup>47, 48</sup> The chemical structures of the products in the CNTs can be directly analyzed using high-resolution transmission electron microscope (TEM) and scanning transmission electron microscopy measurements.

#### 2.2.2 Porous materials

The regular nanochannels of crystalline porous materials can provide unique opportunities to synthesize polymers with controlled structures.<sup>31, 49-51</sup> For example, extensive studies on polymerization in organic crystals have been made from the 1960s to the 1980s. Representative examples include  $\gamma$ -ray-assisted polymerization of conjugated diene and triene monomers in organic hosts, exhibiting specific nanochannel size and shape effects on the kinetics and selectivity of polymerization.<sup>52, 53</sup> Thus, the use of porous materials as hosts is attractive for controlling the polymer structures, as well as the fabrication of novel nanohybrid materials.

#### Mesoporous silicas

Mesoporous silicas are of interest due to their regular frameworks, high surface areas, and remarkable thermal, chemical, and mechanical stabilities. Since the first report on mesoporous silicate MCM-41 in 1992, a variety of mesoporous silicas have been developed.<sup>54</sup> These inorganic materials have uniformly sized mesoscopic channels with an adjustable pore size ranging from approximately 15 to 300 Å. Aida et al. reported polymerization of methyl methacrylate in MCM-41 and showed its potential utility for controlled polymerization.<sup>55</sup> The regular channels of mesoporous silicas can achieve the alignment of polymer chains by the formation of host–guest nanocomposites. Polyacrylonitrile (PAN) was synthesized in the nanochannels of MCM-41, and was subsequently pyrolyzed to form carbonized material.<sup>31</sup> The nanospaces of MCM-41 assisted the formation of larger domains of graphite with ordered structure. As a result, the carbonized material/MCM-41 adduct showed higher microwave conductivity ten times greater than that of the bulk carbon prepared in a similar process. Mesoporous silicas can also be exploited to modulate the optical and electronic properties of confined polymers by controlling the number of polymer chains and their conformation, providing insights for optimizing nanostructured materials for use in optoelectronic devices.<sup>42, 56, 57</sup>

### Metal–organic frameworks

Recently, metal–organic frameworks (MOFs), which are composed of metal ions and bridging organic ligands, have attracted increasing attention as a new class of nanoporous materials.<sup>58–60</sup> Due to their highly regular and well-defined framework structures, MOFs have been applied in numerous fields, including storage and separation, catalysis, sensing, and drug delivery.<sup>61–65</sup> Since the first report on the radical polymerization of styrene in  $[\text{Zn}(\text{bdc})_2\text{ted}]_n$  (bdc = 1,4-benzenedicarboxylate, ted = triethylenediamine) by Uemura et al.,<sup>66</sup> MOFs have been recognized as promising templates for polymerization reactions (Fig. 3).<sup>51, 66–70</sup> The methods for polymerizations generally involve encapsulation of monomers together with the initiators in MOF nanochannels and subsequent heating the resulting composites. Several methods for *in situ*

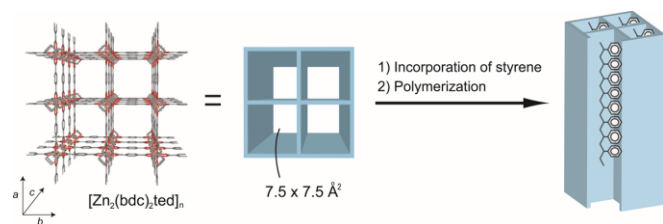


Fig. 3 Schematic illustration of the polymerization of styrene in the nanochannels of  $[\text{Zn}_2(\text{bdc})_2\text{ted}]_n$ . Reprinted with permission from ref. 66. Copyright 2018 Royal Society of Chemistry.

polymerizations have been reported, including radical,<sup>66</sup> oxidative,<sup>71–73</sup> ionic,<sup>74, 75</sup> and ring-opening polymerization,<sup>74, 75</sup> allowing for the production of a highly diverse range of polymers within MOFs.

The design of the framework structures enabled the synthesis of polymers with controlled primary and higher-order structures, such as molecular weight distribution,<sup>66, 76, 77</sup> stereoregularity,<sup>77, 78</sup> alignment,<sup>79, 80</sup> monomer sequences,<sup>81, 82</sup> chirality,<sup>83</sup> and

dimensionalities.<sup>73, 84–88</sup> One of the most important aspects of polymerizations within MOFs is that the monomers fit well in the pores, imposing selective propagation of linear polymer chains. This consideration is very important for monomers with multiple reaction sites. Polymerization of divinylbenzene (DVB) typically resulted in a highly cross-linked insoluble polymer. By contrast, polymerization of DVB in the 1D nanochannels of  $[\text{Zn}_2(\text{bdc})_2\text{ted}]_n$  yielded a completely soluble linear polymer via the selective reaction of only one vinyl group of DVB.<sup>89</sup> The strategies for suppressing cross-linking and branching reactions using MOFs were applied to various types of monomers, including dimethyl 2,2'-[oxybis(methylene)]diacrylate, acrylic anhydride, and 1,6-anhydro- $\beta$ -D-glucose.<sup>74, 90</sup>

It should be noted that the MOF hosts can be easily removed under mild conditions because of the noncovalent framework structures, allowing for the liberation of the polymers without any side reactions during the recovery process. In addition, polymerization by means of MOF templates is tolerant to large-scale operation. These features prompted us to explore the potential of MOFs for precise and scalable synthesis of CLPs described in the next section.

## 3. Synthesis of CLPs from aromatic ring monomers

Considering the chemical structures of CLPs, one can easily imagine that aromatic ring molecules can be utilized as a starting monomer for CLP synthesis. The solubility of aromatic compounds dramatically decreases as the polymerization reactions proceed due to the strong inter-molecular  $\pi$ - $\pi$  interactions. Therefore, ladderization reactions are often incomplete unless elaborate molecular design is applied to improve the reactivity and solubility of the monomers and/or pre-polymers. In this section, we describe the feasible conversion of aromatic ring molecules to CLPs using templates, as well as the unique optoelectronic properties of the CLPs.

### 3.1 Graphene nanoribbons

Graphene nanoribbons (GNRs), nanometer-wide strips of graphene, can be considered one of the most exciting types of CLPs.<sup>91–96</sup> The fascinating electronic and magnetic properties of GNRs are critically defined by the nanoribbon width and edge geometry; thus, fabrication of well-defined GNRs is of great interest to many material scientists. The preparation of GNRs has initially been achieved using “top-down” methods, including unzipping and squashing of the carbon nanotubes and the lithographic cutting of graphenes.<sup>97–99</sup> However, such top-down approaches cannot be used to control over the width and edge structures. In stark contrast, “bottom-up” approaches offer significant opportunities to create atomically precise GNRs. Annulation of precursor polymers in solution can provide GNRs with atomic precision; however, this approach requires the solubilizing substituents, leading to undesirable changes in the intrinsic properties of the GNRs.



The advent of on-surface chemistry has increased the ability to synthesize GNRs without any peripheries. In 2010, Fasel and Müllen et al. developed an elegant approach involving direct growth of GNRs on metal surfaces (Fig. 4a, b).<sup>100</sup> An armchair-edge GNR with a width of seven carbon atoms (7-AGNR) was prepared on Au(111) using 10,10'-dibromo-9,9'-bianthracene (DBBA) as a monomer under UHV conditions. Annealing the surface-deposited DBBA induced a two-step reaction, i.e., thermally initiated dehalogenation at 470 K to yield polyanthracylene intermediates via Ullmann coupling, followed by intrachain cyclodehydrogenation at 670 K to yield 7-AGNR. The formation of 7-AGNR was fully confirmed by high-resolution *in-situ* STM analysis.<sup>100</sup> The on-surface reaction mechanism of the GNR was investigated by theoretical calculations.<sup>101</sup> It was found that the Au(111) surface catalyzed the Ullmann coupling and cyclodehydration reactions: two H-atoms from anthracene units were pulled onto the surface, followed by desorption into the vacuum. The cyclodehydration reaction started at one end of the polyanthracene chain with a domino-like effect, where steric hindrance plays a key role.

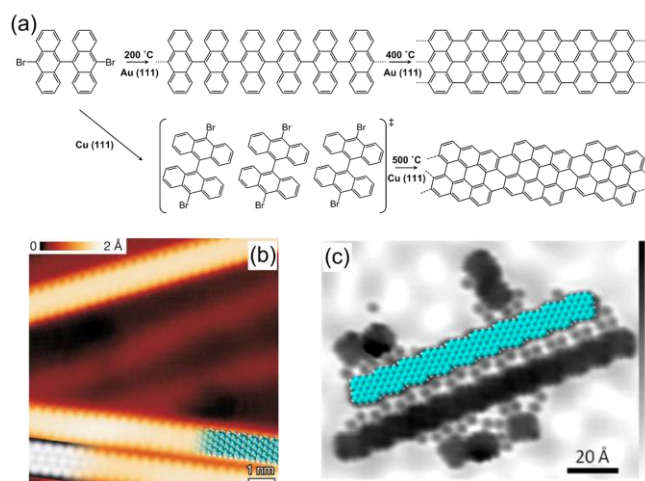


Fig. 4 (a) On-surface synthesis of 7-AGNR and (3,1)-chiral GNR. (b, c) STM images of (a) 7-AGNR on Au(111) and (c) (3,1)-chiral GNR on Cu(111). (b) Reprinted with permission from ref. 100. Copyright 2010 Macmillan Publishers Ltd. (c) Reprinted with permission from ref. 109. Copyright 2013 American Chemical Society.

The accessible amount of GNRs is limited to areas smaller than 1 cm<sup>2</sup> under UHV conditions due to the small size of the UHV chamber. Elaborate and costly UHV equipment limits efficient fabrication of GNRs. By employing the readily available chemical vapor deposition (CVD) technique, Sakaguchi et al. developed an efficient process for high-throughput synthesis of atomically precise GNRs (Fig. 5).<sup>102</sup> The resulting 7-AGNR could be transferred from metal to an insulating substrate for device fabrication and exhibited a significant photocurrent higher than that of a conventional p-type semiconductor, poly(3-hexylthiophene). Samori et al. fabricated a field-effect transistor (FET) memory device with a MoS<sub>2</sub>/7-AGNR van der Waals heterostructure.<sup>103</sup> 7-AGNR withdraws the redundant electrons from the intrinsically n-doped MoS<sub>2</sub>, suppressing the remaining photoconductivity after the termination of illumination.

The effective interfacial charge transfer process achieved the photomodulation of the source drain current up to 52%. These results demonstrate the potential of AGNRs as a promising photoactive layer.

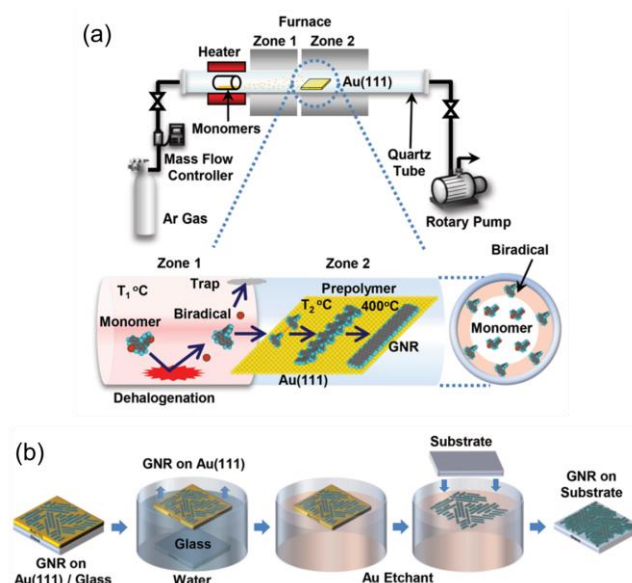


Fig. 5 (a) Experimental CVD setup with an illustration of the GNR growth mechanism using DBBA. (b) Schematic illustration of GNR transfer process from the metal to the insulating substrate. Reprinted with permission from ref. 102. Copyright 2014 Wiley.

Many types of GNR structures, including AGNRs<sup>102, 104-108</sup>, chevron-type GNRs,<sup>100</sup> chiral GNRs,<sup>109-112</sup> hetero-atom-doped GNRs<sup>113-115</sup>, and heterojunctions<sup>116-120</sup> have been successfully synthesized on metal surfaces. In contrast, the synthesis of zigzag-edge GNR (ZGNR) has been significant challenge because the aryl-aryl coupling of monomers does not take place along the zigzag direction. Recently, the use of a U-shaped monomer has enabled the synthesis of a ZGNR featuring six carbon atoms across the width of the ribbon (6-ZGNR).<sup>121</sup> After polymerization of the U-shaped monomer on Au(111), the obtained pre-polymers were further annealed to initiate the cyclodehydration reaction. The methyl groups were dehydrogenatively incorporated to form a fully conjugated system with zigzag edges (Fig. 6). To decouple the electronic interaction between the GNRs and the metal surface, as-synthesized GNRs were transferred to insulating NaCl islands. Evidence for the theoretically predicted edge states of the ZGNRs was obtained from the *dI/dV* spectrum taken at the edge of 6-ZGNR. ZGNRs can be doped by hetero atoms in their zigzag edges for novel magnetic properties. Fischer et al., fabricated a nitrogen-doped 6-ZGNR (6-nZGNR), in which every sixth C–H group along the edge was replaced by a nitrogen atom.<sup>122</sup> STS measurements of 6-nZGNR revealed a significant splitting of the dopant edge state induced by the ferromagnetically ordered spins along the edge in agreement with theoretical calculations. The use of 6,11-bis(10-bromoanthracen-9-yl)-1,4-dimethyltetracene and DBBA as a monomer provided a heterojunction of GNRs with armchair and zigzag edges via the oxidative cyclization of methyl groups.<sup>117</sup> Strikingly, the topological end states were demonstrated at their

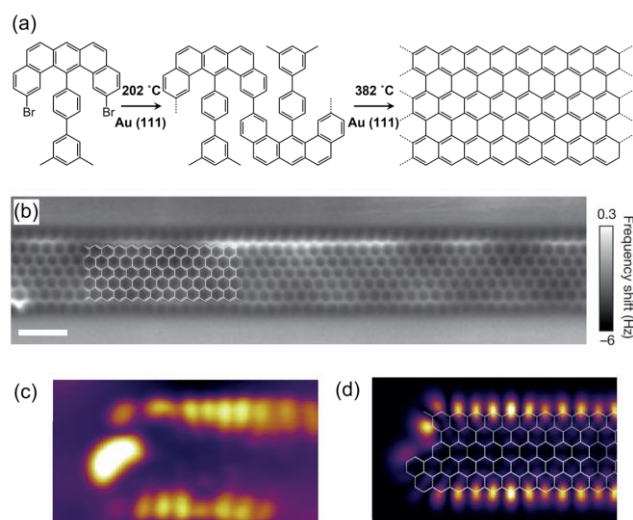


Fig. 6 (a) Synthetic route for 6-ZGNR. (b) STM image of 6-ZGNR on Au(111). (c) Differential conductance maps of filled edge states taken at a sample bias of 0.3 V. (d) DFT-based local density of states at a 4-Å tip-sample distance, showing the spatial distribution of filled edge states. Reprinted with permission from ref. 121. Copyright 2016 Macmillan Publishers Ltd.

interfaces by  $dI/dV$  mapping, suggesting the significant potential of GNRs as a platform for developing topological quantum materials.

Along with the monomer design, the choice of substrate also has a significant effect on the selectivity of a target reaction. Interestingly, on Cu(111), a (3,1)-chiral GNR was formed using the same monomer through selective dehydrogenative coupling at the 2,2'-sites of DBBA (Fig. 4a, c).<sup>109</sup> In the case of 7-AGNR synthesis on Au(111), the biradical intermediates are mobile, which allow them to find the active reaction site.<sup>123</sup> In contrast, the DBBA monomers on Cu(111) cannot diffuse freely even at elevated temperatures. As a result, the cyclodehydrogenation reaction only occurs inside preassembled domains.

In general, the length of GNRs synthesized on surfaces is limited by the undesired hydrogen passivation reaction of the radical ends of the oligomers and/or surface defects and step edges.<sup>124</sup> The short lengths make it difficult to connect the GNRs to metal electrodes for their integration into molecular-based devices. The use of monomers with different halogen functionalization units revealed the impact of halogen atoms on the GNR length. The use of iodine-containing monomers induced the growth of longer AGNRs (average length = 45 nm) in comparison with the analogue containing a bromine group (average length = 15 nm).<sup>125</sup> Iodine has a higher desorption temperature from metal surfaces than that of bromine, promoting the formation of hydrogen iodide after the release of hydrogen atoms from the cyclodehydration process, which restrains the undesirable termination reaction of the active terminus.

Supramolecular interactions of building units enabled the control of inter-chain coupling reactions, as demonstrated by the synthesis of 7-AGNR using para-dibromoterphenylene (DBTP) as a monomer.<sup>126</sup> The halogen atoms in monomer units play a key role in their well-organized structures. The DBTP monomers were perfectly

aligned on the Au(111) surface by halogen bond interactions between the monomers (Fig. 7a–d). The first annealing process led to debromination and the formation of polyphenylene chains. The pre-alignment of DBTP served as a template to guide the dense alignment of polyphenylene. Finally, higher temperature annealing induced the formation of the perfectly aligned fused nanoribbons. Recently, Moreno et al. successfully synthesized an aligned GNR with a length of > 100 nm using a reconstructed Au (111) surface (Fig. 7e, f).<sup>127</sup> The uniaxial anisotropy of the zigzag pattern of the surface directed the growth of the GNR. The engineering of surface topologies would contribute to the realization of the parallel arrays of long GNRs that are essential for improving the performance of nanodevices.

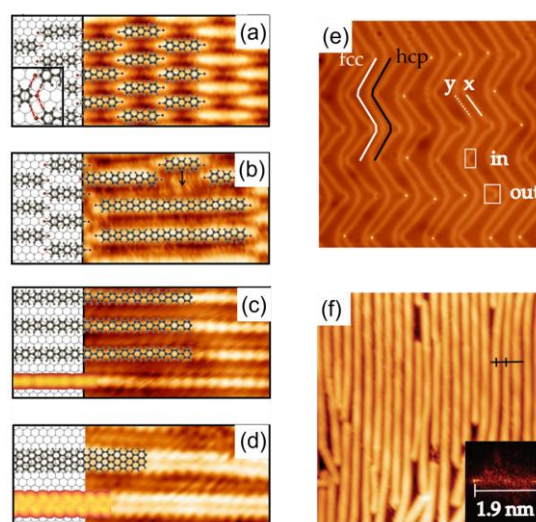


Fig. 7 (a–d) In-situ STM images during formation of 7-AGNR using DBTP as a monomer. Annealing at (a) 47, (b) 87–127, (c) 247, and (d) 377 °C, respectively. Alignment of the DBTP monomers was preserved during the annealing process and stepwise formation of aligned polyphenylene chains and the GNR. (e–f) STM images of (e) Au(111) surface consisting of a periodic array of face-centered-cubic (fcc) and hexagonal-close-packed (hcp) stacking strip domains and (f) the GNRs. Fourier transform of the STM image (inset) clearly shows the periodically ordered structures. (a–d) Reprinted with permission from ref. 126. Copyright 2015 American Chemical Society. (e–f) Reprinted with permission from ref. 127. Copyright 2018 Royal Society of Chemistry.

Recent works demonstrated that the on-surface method is suitable for fabricating 2D nanoporous GNRs in a programmable manner.<sup>128–131</sup> A 2D GNR network was synthesized on a reconstructed Au(111) surface, in which the surface-assisted parallel alignment of a cross-linkable GNR is essential for the efficient interchain cross-linking reaction (Fig. 8).<sup>129</sup> The 2D nanoporous GNR showed a localized electronic state within the pores with a Fermi level that can be shifted by the interaction with ions and molecules, making this GNR a promising material for chemical and biological sensors. A short-channel field-effect transistor (FET) device was fabricated using a chevron type 2D GNR, and exhibited excellent switching behavior with superior on-off ratios of  $10^4$ , in comparison with those of graphene.<sup>131, 132</sup> Interestingly, the FET device exhibited n-type

charge transport behavior under vacuum while the device in air converted to a p-type transistor. These device behavior changes are attributed to the absorption of gases or moisture that induced changes in the electronic band structures.

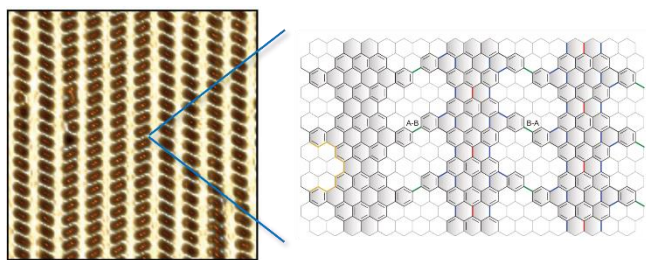


Fig. 8 Laplacian-filtered topographic image of nanoporous graphene. Reprinted with permission from ref. 129. Copyright 2018 AAAS.

The aforementioned bottom-up strategies using surface-mediated chemical reactions were confirmed to be effective for synthesizing GNRs with atomic precision, although in extremely small quantities due to the limited available reaction areas on the substrates. In recent years, the use of the 1D nanospaces of CNTs and porous materials provided an effective method for the scalable and precise synthesis of GNRs.

Talyzin et al. demonstrated that perylene could be polymerized and fused into an AGNR with a width of five carbon atoms (5-AGNR) by heat treatment within a single-walled CNT (SWCNT), as confirmed by Raman and TEM measurements (Fig. 9).<sup>28</sup> The diameter of the host SWCNT is critical for the orientation of the guest species, dictating the reactivity of the monomers, as well as the chemical structures of the polymers. First-principle simulations showed that encapsulation of the GNRs in the SWCNT with a diameter of 1.4 nm was energetically favorable with respect to the isolated systems, facilitating the formation of the GNRs within SWCNTs.<sup>28</sup> In a similar manner, the synthesis of GNRs in SWCNTs has been reported using a fullerene derivative, tetrathiafulvalene, and perylene-3,4,9,10-tetracarboxylic dianhydride as precursors.<sup>133-135</sup> The zigzag edges of the nanoribbons were terminated with sulphur atoms generated from the precursors, stabilizing otherwise unstable GNRs.<sup>133, 134</sup> Thermally induced self-intertwining of the resulting GNRs led to the selective formation of CNTs with specific chirality in the parent-tube templates, which appeared a promising route for the synthesis of well-defined CNTs.<sup>135</sup>

Owing to the exceptionally high stability of CNTs, the removal of host CNTs remains challenging. Thus, isolation of the GNRs has never been achieved, limiting further study and applications of the GNRs; instead, much attention has been given to the properties of the GNRs inside the nanotubes. The electronic structures of CNTs can be modulated by surface covalent functionalization. Suppression of the excitonic absorption peaks of the nanotubes enabled the investigation of the optical properties of the GNRs in the nanotubes.<sup>136</sup> Khlobystov et al. revealed the diverse dynamic behavior of the GNRs within the SWCNTs, in which rotation, translation, and helical twisting motions were observed (Fig. 10).<sup>134</sup> Since the physical properties of the GNRs would be significantly affected by the GNR conformations,<sup>137, 138</sup> this finding shows promise

for the control of the electronic and magnetic properties of GNRs via nanoconfinement. Furthermore, this method can provide a route for the fabrication of novel carbon nanocomposites with superior optoelectronic properties beyond those offered by the individual components. The electronic structures of CNT/GNR nanohybrids

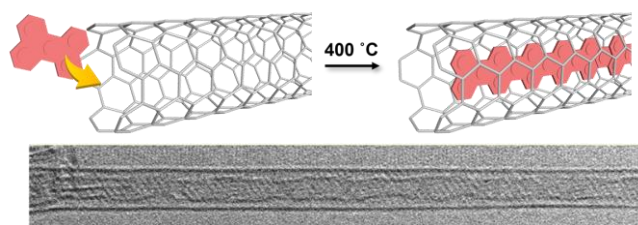


Fig. 9 Schematic image for 5-AGNR synthesis in SWCNT using perylene as a monomer and TEM image of SWCNT containing 5-AGNR. Reprinted with permission from ref. 28. Copyright 2011 American Chemical Society.



Fig. 10 TEM images of GNRs with different widths inside nanotubes. Reprinted with permission from ref. 134. Copyright 2012 American Chemical Society.

have been studied theoretically, demonstrating that the nanohybrids form a type-II heterojunction and charge transfer occurs in opposite directions at the interface.<sup>139</sup> Well-separated spatial distribution of electrons and holes make this class of nanohybrids promising for photovoltaic and electronics applications.

Preparation of properly engineered nanospaces with controlled sizes is an essential prerequisite for the precise synthesis of GNRs. Owing to their design freedom and diverse functionality, MOFs can provide an ideal reaction field for GNR synthesis. Uemura and co-workers have recently disclosed a new method for bulk-scale synthesis of GNRs with atomic precision using a MOF as a template. The first report on GNR synthesis in MOFs involved the synthesis of 5-AGNR within the 1D nanochannels of  $[\text{ZrO}(4,4'\text{-biphenyldicarboxylate})]_n$  via the selective coupling reaction of perylene (Fig. 11).<sup>29</sup> The coupling reaction of perylene does not proceed at 400 °C in the bulk state. An increase in the heating temperature to 600 °C led to the formation of branched or graphitic structures. Strikingly, the polymerization of perylene proceeded within the MOF even at 400 °C, most likely because the Lewis acid sites in the MOF acted catalytic sites<sup>140</sup> and/or the perylene molecules aligned uniaxially along the nanochannels. As a result, 5-AGNR formed via the selective coupling reaction at the 3-, 4-, 9-, and 10-positions of perylene. The bulk quantity of 5-AGNR could be obtained by digesting the framework, as evidenced by a series of characterization methods, including Raman, NMR, IR, and MALDI-TOF MS measurements. The careful selection of host and monomer



combinations will accomplish the fabrication of a variety of GNRs. Bulk-scale GNRs enable a wide range of methods for evaluating the chemical and physical properties of GNRs, as well as their practical applications in electronics.

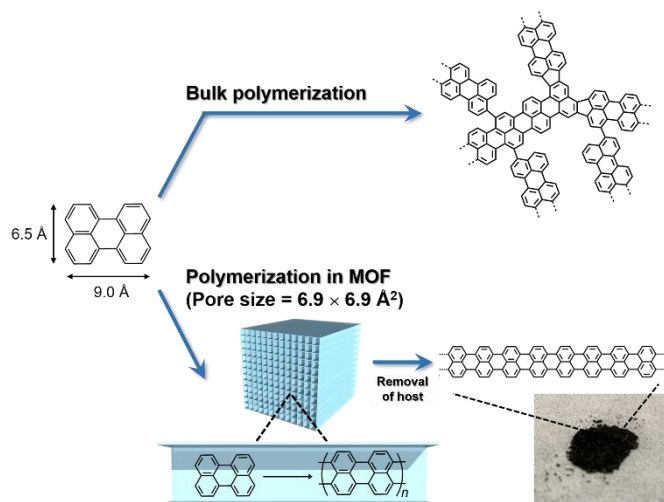


Fig. 11 Schematic of the fabrication of 5-AGNR with atomic precision on the bulk scale using a MOF as a template. Reprinted with permission from ref. 29. Copyright 2020 American Chemical Society.

In addition to their width and edge structures, interchain interactions are also important in governing a diverse range of GNR properties and functions. Thus, it is essential to control the assembly packing structures of GNRs at the molecular level. However, strong interchain  $\pi$ - $\pi$  interactions cause GNRs to be non-melting and insoluble; hence the control of the assemblies has remained challenging, thus significantly limiting the extensive application of GNRs. Since host MOFs can be removed under mild conditions, polymer assemblies can be retained even after the removal of the frameworks.<sup>79, 80</sup> MOF-templated methods would provide the highly ordered alignment of the nanoribbons, leading to the enhancement of their functions for future application in FETs and photovoltaic cells.

Recently, the surface-confined preparation of 2D nanoporous GNRs on metal substrates has been reported.<sup>129, 131</sup> However, this method requires highly symmetric multivalent monomers to define the growth and dimensions of the networks. In addition, this surface-assisted method inevitably suffers from their scalable synthesis. Dimensionally programmed polymerization in the 2D nanospaces of MOFs<sup>84</sup> will afford 2D GNRs with precise structures and scalability, leading to the expression of the topological properties.<sup>141</sup>

### 3.2 CLPs comprising nonbenzenoid moieties

In non-benzenoid systems, the  $\pi$ -electron density distribution and molecular orbital levels are uneven in contrast to those of benzenoid systems, polarizing the ground state and leading to intriguing behavior in the excited state.<sup>142</sup> The incorporation of nonbenzenoid rings into CLPs represents another approach for significantly modulating CLP properties. CLPs containing nonbenzenoid components are theoretically predicted to exhibit an open-shell state

with one or more unpaired electrons, leading to characteristic physicochemical properties, such as narrow Highest Occupied Molecular Orbital-Lowest Occupied Molecular Orbital gaps and anti-aromaticity.<sup>143, 144</sup> CLPs synthesized by incorporating nonbenzenoid moieties in wet chemistry suffer from structural defects and low solubility that prevent control over the synthesis as well as structural characterization at the atomic level.

Ladder phenylene (LP) is comprised of linearly alternating fused benzene and cyclobutadiene rings. LPs are expected to possess intriguing optoelectronic properties due to this combination of aromatic and antiaromatic groups.<sup>145</sup> Despite many efforts to synthesize LPs in solution, the longest LPs contained only five benzene units because of their insolubility and poor stability, which limited the exploration of the properties of the polymeric LP.<sup>146</sup> Liu et al. reported the synthesis of LP with more than 50 units on Au(111) by direct ladder polymerization, surface-assisted debrominative [2+2] cycloaddition; noncovalent interactions of the methyl groups of 1,2,4,5-tetrabromo-3,6-dimethylbenzene (TBDMB) improve the chemoselectivity and the orientation orderliness (Fig. 12).<sup>147</sup> The electronic properties of LP were examined by scanning tunnelling spectroscopy (STS) measurements after transferring the LP chains from the metal surface to NaCl islands via tip manipulation. LP was found to be positively charged, with singly occupied (SOMO) and associated unoccupied (SUMO) molecular orbitals identified by  $dI/dV$  maps and confirmed by density functional theory (DFT) calculations. Although LP was predicted to show an antiferromagnetic ground state by the DFT calculations, no obvious spin excitation has been seen in  $dI/dV$  spectra. This is probably because the magnetization would be affected by multiple factors, such as substrate screening effects, adsorption configurations, and charge transfer. Various types of CLPs containing cyclobutadienoid moieties have been synthesized by means of debrominative [2+2] cycloaddition, and they exhibited unique optoelectronic properties.<sup>148, 149</sup> For example, a linearly fused coronene-cyclobutadienoid polymer featured an exceptionally narrow indirect band gap of 600 meV.<sup>148</sup>

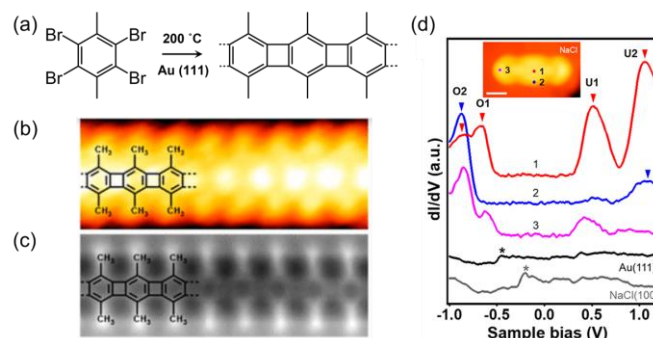


Fig. 12 (a) Synthetic route for LP using TBDMB as a monomer. (b) STM image of LP. (c) STM image of LP. (d)  $dI/dV$  spectra recorded on different locations of LP (marked in the inset STM image). Chemical structure of poly(indenoindene). The two states (O1 and U1) were assigned as the SOMO and SUMO, respectively. Reprinted with permission from ref. 147. Copyright 2021 American Chemical Society.

Poly(indenoindene) is a CLP consisting of an alternating sequence of five- and six-membered rings. The synthesis of poly(indenoindene)



has remained challenging to date because of the inherent reactivity of the indenofluorene monomers.<sup>150</sup> The on-surface method enabled the synthesis of poly(indenoindene) by sequential aryl–aryl coupling of the *p*-terphenyl-based precursor and oxidative cyclization of methyl groups against the phenylene rings of the polyphenylene

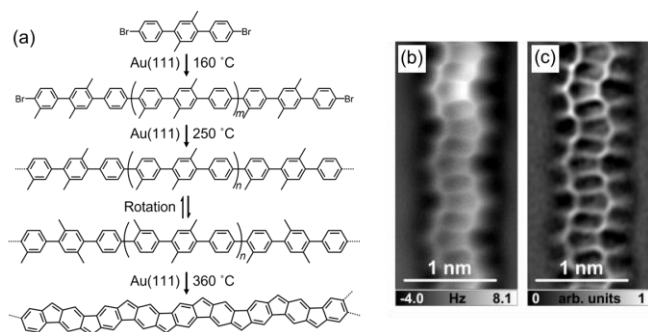


Fig. 13 (a) Reaction pathway from *p*-terphenyl-based precursor to poly(indenoindene). (b, c) AFM (b) and Laplace-filtered (c) images of poly(indenoindene) synthesized on Au (111). Reprinted with permission from ref. 151. Copyright 2020 American Chemical Society.

backbone (Fig. 13a-c).<sup>151</sup> The successful “zipping” of the pre-polymer was confirmed by STM and AFM measurements. The DFT calculations and STS measurements revealed the low band gap and antiferromagnetic character of poly(indenoindene).

The incorporation of fused pentalene units into CLPs was achieved by Ćcija et al. Ethynylene-linked anthracene and cumulene-linked bisanthracene polymers were synthesized on Au(111) using [9,10-bis(dibromomethylene)-9,10-dihydroanthracene] (4BrAn) and [10,10'-bis(dibromomethylene)-10H,10'H-9,9'-bisanthracenyliene] (4BrBIA) as a monomer, respectively (Fig. 14).<sup>152</sup> Interestingly, despite their similar cyclization activation barriers, annealing of the precursor polymers led to distinct behavior of the formed polymers. In the case of the anthracene polymers, the annealing process induced distinct side reactions, giving rise to intra-polymeric warping and inter-polymeric fusion. In contrast, thermal treatment of the bisanthracene polymer resulted in the formation of a non-benzenoid fused pentalene bridged CLP via a two-fold cyclization reaction. The observed differences in reactivity were rationalized in terms of the vibrational modes of the polymers; the bending vibration modes of the bisanthracene polymer matched very well with the cyclization reaction coordinate. High resolution AFM images allowed identification of the resonance form of the polymer, demonstrating the Glidewell and Lloyd rules for aromaticity.<sup>153, 154</sup>

Azulene consists of annulated five- and seven-membered rings. CLPs containing four-, five, and seven-membered rings were obtained using polyazulene chains as a precursor polymer.<sup>155</sup> Initially, polymerization of 2,6-dibromoazulene was performed on the Au(111) surface by Ullmann coupling, leading to ordered domains of polyazulene chains. During the polymerization, bromine adatoms were generated by C–Br bond scission of the monomer. The resulting Br...H hydrogen bonds are the driving force for the ordered arrangement of the polymer chains. Finally, the lateral dehydrogenative C–C coupling of the neighboring polyazulene chains led to the formation of CLPs containing four-, five, and seven-membered rings.

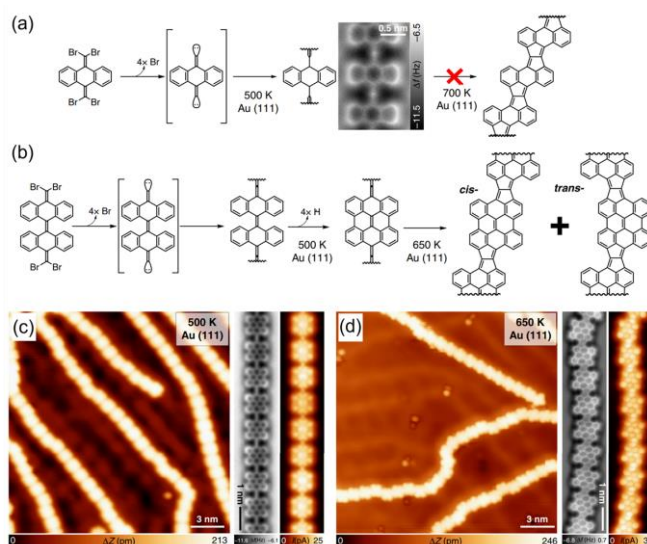


Fig. 14 (a, b) Scheme of the reaction sequence of (a) 4BrAn and (b) 4BrBIA. (c, d) STM image of (c) bisanthracene polymer and (d) fused pentalene bridged CLP. Reprinted with permission from ref. 152. Copyright 2020 Macmillan Publishers Ltd.

Eight-membered rings were also periodically incorporated into the structures of CLPs. 1,6,7,12-tetrabromo-3,4,9,10-perylene-tetracarboxylic-dianhydride (Br<sub>4</sub>-PTCDA) was sublimed onto the Au(111) surface as a monomer (Fig. 15).<sup>156</sup> In addition, 4,4''-dibromo-*p*-terphenyl (DBTP) molecules were codeposited with Br<sub>4</sub>-PTCDA. Owing to the instability of the anhydride groups of Br<sub>4</sub>-PTCDA, undesirable reactions, such as decarbonylation and ring opening reactions of anhydrides may take place, leading to disordered structures. DBTP first reacted after annealing to form polyphenylene,

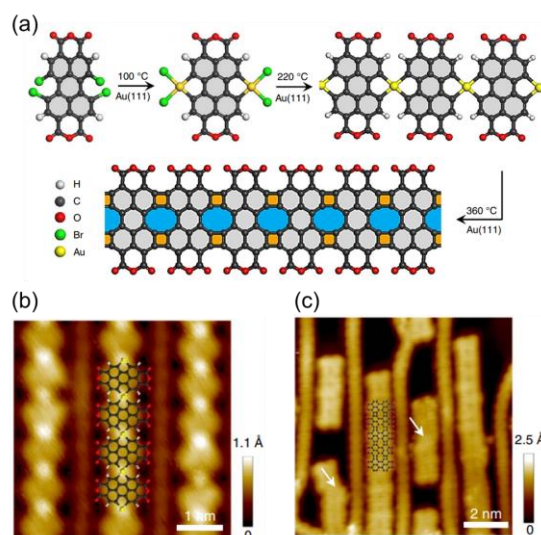


Fig. 15 (a) Synthetic strategy for CLPs containing eight- and four-membered rings. (b) STM image of PTCDA-Au<sub>2</sub>-Br<sub>4</sub> linear chains. (c) STM image of CLP periodically embedded with eight- and four-membered rings. Reprinted with permission from ref. 156. Copyright 2017 Macmillan Publishers Ltd.

which served as 1D molecular grooves to constrain Br<sub>4</sub>-PTCDA, preventing such side reactions. Thermal annealing of Br<sub>4</sub>-PTCDA induced the C–Br bond cleavage and the PTCDA intermediates diffused unidirectionally along the molecular grooves, yielding PTCDA-Au<sub>2</sub>-Br<sub>4</sub> linear chains. Further annealing released gold atoms from the polymers, resulting in the regulated formation of eight- and four-membered rings between perylene backbones.

CLPs consisting of repeated porphyrin units, so-called porphyrin nanotapes<sup>157, 158</sup>, have also gained considerable attention as near-infrared absorbers and molecular wires. The on-surface approach provided porphyrin nanotapes and atomic-scale characterizations of their structural and electronic properties (Fig. 16).<sup>159</sup> Porphyrin nanotapes provide a scaffold for the arrangement of magnetic ions using the inner porphyrin cavity, which would lead to exotic physical phenomena and quantum applications.

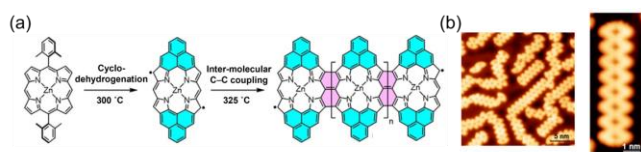


Fig. 16 (a) Two-step strategy for synthesis of laterally  $\pi$ -extended porphyrin nanotapes on Au(111). (b) STM images of porphyrin nanotapes. Reprinted with permission from ref. 159. Copyright 2021 Wiley.

#### 4 Synthesis of CLPs by zipping of vinyl polymers

Carbon fibers have been a critical engineering material since their initial development in the 1960s because of their outstanding physical properties.<sup>160</sup> PAN is one of the most widely used precursors for carbon fibers. Among the several production processes, thermal stabilization is the most important process for obtaining fine carbon fibers, in which PAN transforms into a nZGFR featuring two lines of carbon atoms across the width of the ribbon (2-nZGFR) via intrachain cyclization and dehydration reactions.<sup>161</sup> However, a series of characterization methods demonstrate that the actual structure of 2-nZGFR is more complex and consists of cross-linking, aliphatic carbon, and carbonyl groups. It is crucial to control the ladderization (zipping) reaction; however, both intra- and interchain reactions inevitably occur in the bulk state because of the random polymer entanglement. Furthermore, the stabilization is an exothermic reaction with an abrupt heat release that causes many side reactions, such as chain scission, resulting in the complicated and uncontrollable structure of the product.

Confinement of polymer chains in porous materials is a feasible method for controlling polymer assemblies because this approach can prevent the entanglement and conformational disorder of polymer chains in the bulk state. Nanoconfinement effects on the reactivity of PAN have been extensively explored using nanoporous materials. Initially, PAN was prepared by *in-situ* polymerization of acrylonitrile, then subsequently pyrolyzed inside the channels of MCM-41 with a pore size of ca. 30 Å.<sup>31</sup> The obtained carbon nanofilaments had well-ordered graphitic domains and showed higher microwave conductivity than that of the bulk PAN pyrolyzed

under the same conditions. This was probably owing to the polymer chain alignment within the 1-D nanochannels that facilitate the stabilization and carbonization reactions. Recent studies showed that the stabilization reaction of PAN was radically affected by the environment surrounding the polymer chains because of the isolated chain state. The stabilization reaction of PAN proceeds with abrupt heat release, as observed by the sharp exothermic peak around 280 °C in the differential scanning calorimetry (DSC) curve for the neat PAN.<sup>161</sup> The stabilization reactions of PAN confined in porous materials were examined using DSC measurements. The transformation temperature of PAN within the 3-D porous polymer (pore size = 14 Å) was shifted 20 °C higher than that of the neat PAN.<sup>48</sup> This was most likely because the polymer chains were strictly interwoven within the 3D host and the kinetics of the transformation slowed. In contrast, the transformation temperature of PAN within the 1D channels of mesoporous organosilica (pore size = 38 Å) was 40 °C lower than that of neat PAN because of an extended conformation of PAN chains within the channels that promoted the intramolecular cyclization process.<sup>49</sup>

The controllable channel size of MOFs enables the achievement of precise polymer assemblies in the nanochannels, which are of key importance for inhibiting the interchain cross-linking reactions of

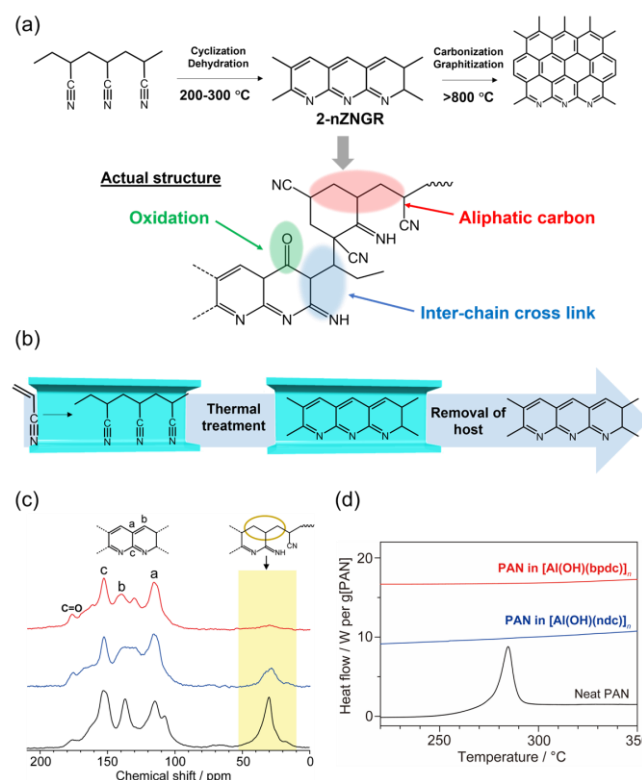


Fig. 17 (a) Scheme of chemical reaction for carbon fibers. (b) Schematic for the transformation reaction of PAN within the nanochannels of MOFs. (c) Solid-state <sup>13</sup>C NMR spectra of neat PAN after heating at 280 °C (black) and 2-ZGFR liberated from [Al(OH)(bpdcl)]<sub>n</sub> (red) and [Al(OH)(ndc)]<sub>n</sub> (blue). (d) DSC curves of neat PAN, PAN in [Al(OH)(bpdcl)]<sub>n</sub>, and PAN in [Al(OH)(ndc)]<sub>n</sub>. Reprinted with permission from ref. 30. Copyright 2020 Royal Society of Chemistry.

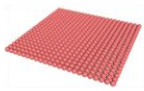
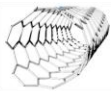


	Metal surface	CNT	Mesoporous silica	MOF
				
Modularity/diversity	Good	Good	Good	Excellent
Order/crystallinity	Excellent	Excellent	Average	Excellent
Uniformity	Excellent	Generally bad; current methods produce mixture of CNTs with varying diameters	Average	Excellent
Thermal and chemical stability	Excellent	Excellent	Excellent	Can be good through choosing appropriate metal ions and ligands
Structural characterization of CLPs	Excellent; direct observation methods (e.g. STM and AFM) can be used.	Good; structures can be analyzed using TEM.	Good; structures can be analyzed using diverse characterization methods (e.g. NMR, IR, and MALDI-TOF MS).	Good; structures can be analyzed using diverse characterization methods (e.g. NMR, IR, and MALDI-TOF MS).
Characterization of physical properties of CLPs	Average; electronic coupling with metals would change intrinsic properties of CLPs.	Average; electronic coupling with CNTs would change intrinsic properties of CLPs.	Can be good; electronic coupling with mesoporous silicas might be changed by pore surface modifications.	Good; electronic coupling with MOFs can be modulated using electrically inactive hosts.
Scalability of CLPs	Tiny amount	Can be good, but CLPs cannot be isolated from CNTs	Can be good, but harsh conditions are required for removal of hosts	Excellent; bulk quantity of CLPs can be obtained by digesting hosts under mild conditions

Fig. 18 Characteristic features of metal surfaces, CNTs, mesoporous silicas, and MOFs for CLP synthesis.

PAN. We performed the transformation reaction of single PAN chains within two MOFs with distinct channel sizes,  $[Al(OH)(bpdC)]_n$  (pore size = 11.1 Å) and  $[Al(OH)(ndc)]_n$  (ndc = 2,6-naphthalenedicarboxylate, pore size = 8.5 Å) to study the effect of pore size on the transformation process (Fig. 17a, b).<sup>30</sup> Note that the 2-nZGNR prepared within the MOFs had a more extended conjugated backbone with smaller amounts of aliphatic carbons than in the bulk condition, as confirmed by solid-state <sup>13</sup>C NMR (Fig. 17c). Accommodation of single PAN chains in MOF nanochannels allowed for the suppression of rapid heat generation during the stabilization process (Fig. 17d). In general, MOFs show low thermal conductivity because of the heterogeneity of the bond stiffnesses and atomic masses.<sup>162</sup> PAN chains were encapsulated within each nanochannel in a single-chain fashion. Thus, heat transfer between the polymer chains was inhibited, suppressing the abrupt heat release. Further heat treatment of 2-nZGNR will potentially enhance the properties of the carbon fibers. Owing to the extended conjugated backbone with a heteroatom-doped structure, the formation of 2-nZGNR within the MOFs would result in fascinating physicochemical properties.

The molecular weight, primary structures, and loading amounts of the precursor polymers would significantly affect the structures and properties of the CLPs after the zipping reaction. However, with the *in situ* polymerization method, this level of precise control remains challenging. In 2010, it was demonstrated that polyethylene glycol (PEG) spontaneously intercalated into nanopores when mixed with MOFs above its melting temperature.<sup>163</sup> Moreover, Uemura *et al.* have recently demonstrated that the insertion of PEG into MOFs occurred even in the solution phase.<sup>164, 165</sup> Due to their flexible main

chains, the control of ladderization reactions of vinyl polymers has remained challenging, and there are limited examples of CLPs and non-conjugated ladder polymers. The direct insertion of precursor vinyl polymers with well-defined primary structures into MOFs will allow a much wider scope of ladder polymers with well-defined structures and novel topological properties.

#### 4. Summary and outlook

For the synthesis of CLP, the development of synthetic strategies in solution has seen significant progress. However, this conventional method suffers from the formation of undesirable non-ladder defects (e.g. cross-linking and branching) owing to the multiple reaction sites. The difficulty in precision chemical synthesis as well as solubility issues in synthesis, characterization, and processing should be overcome for their future applications.<sup>166</sup> In this review article, we described the progress of CLP synthesis using various templates. As shown in Fig. 18, this approach has some general advantages and disadvantages. Thus, the appropriate choice and rational design of the templates are required for the synthesis and applications of targeted CLPs. Although this methodology affords a wide range of CLPs that cannot be produced using conventional solution approaches, there are still many scientific and technological challenges that must be overcome for their future applications.

The intrinsic high density of low-energy electronic states of a metal substrate does not allow for the electronic decoupling of the synthesized CLPs, which is essential for detailed characterizations of their intrinsic properties, such as conductivity and magnetism.

Furthermore, these obstacles hinder the applications of CLPs with unique physicochemical functions in electronic and magnetic devices.<sup>167</sup> The synthesis of CLPs on nonmetals (such as insulators or semiconductors) is difficult because the metal surfaces act as a polymerization catalyst. The transfer of the polymers onto nonmetal substrates is complex and time-consuming. Therefore, the exploration of direct fabrication methods on nonmetal substrates is greatly needed.<sup>168, 169</sup> A combination of STM with an optical detection system<sup>170</sup> allows for the exploration of the optical properties of CLPs at the atomic scale, providing a deeper insight for future design and optimization of molecular-scale devices.

The current fabrication methods, such as arc discharge and chemical vapor deposition, typically produce CNTs with various diameters and sidewall structures (armchair, zigzag, and chiral).<sup>171</sup> Improvements in CNT synthesis will result in greater control of nanotube structures,<sup>172</sup> allowing the specific selection of CNTs for the control of polymerization reactions.

Because of their high degree of design freedom, the use of MOF templates can satisfy the requirement of both precision at the atomic scale and scalability. From the viewpoint of polymer synthesis, periodic incorporation of catalytically active metal sites in the frameworks will facilitate the formation of CLPs within nanochannels, expanding the scope of CLP synthesis. In addition, nanoconfinement of the polymer chains within the nanochannels will endow the CLPs with new functions via electronic and magnetic couplings between host and guests.<sup>83, 173-175</sup> One of the most striking features of MOFs is their flexibility, by which the frameworks undergo structural changes upon exposure to external stimuli, such as heat, light, pressure, and magnetic fields. Cooperative structural transformations of MOFs and CLPs will offer opportunities for fabrication of novel stimuli-responsive materials, which are highly beneficial for optoelectrical applications.

Overall, recent rapid progress in the confined synthesis of CLPs has led to breakthroughs in both fundamental science and materials applications. We envision that the demand for novel CLPs will increase more than ever in the near future, and believe the development of new templates will guide the more thrilling discoveries in this class of polymeric nanomaterials.

## Acknowledgements

This work was supported by JST-CREST (JPMJCR20T3) and JST-PRESTO (JPMJPR21A7) programs, and a Grant-in-Aid for Scientific Research (21H01738 and 21H05473) from the Ministry of Education, Culture, Sports, Science and Technology, Government of Japan.

## References

- U. Scherf, *J. Mater. Chem.*, 1999, **9**, 1853-1864.
- L. Yu, M. Chen and L. R. Dalton, *Chem. Mater.*, 1990, **2**, 649-659.
- J. Lee, A. J. Kalin, T. Yuan, M. Al-Hashimi and L. Fang, *Chem. Sci.*, 2017, **8**, 2503-2521.
- A.-D. Schlüter, *Adv. Mater.*, 1991, **3**, 282-291.
- Z. Cao, M. Leng, Y. Cao, X. Gu and L. Fang, *J. Polym. Sci.*, 2022, **60**, 298-310.
- A. Narita, X.-Y. Wang, X. Feng and K. Müllen, *Chem. Soc. Rev.*, 2015, **44**, 6616-6643.
- J. Wu, X. Rui, C. Wang, W.-B. Pei, R. Lau, Q. Yan and Q. Zhang, *Adv. Energy Mater.*, 2015, **5**, 1402189.
- C.-Y. Yang, M.-A. Stoeckel, T.-P. Ruoko, H.-Y. Wu, X. Liu, N. B. Kolhe, Z. Wu, Y. Puttisong, C. Musumeci, M. Massetti, H. Sun, K. Xu, D. Tu, W. M. Chen, H. Y. Woo, M. Fahlman, S. A. Jenekhe, M. Berggren and S. Fabiano, *Nat. Commun.*, 2021, **12**, 2354.
- Y. Chen, H. Li, M. Tang, S. Zhuo, Y. Wu, E. Wang, S. Wang, C. Wang and W. Hu, *J. Mater. Chem. A*, 2019, **7**, 20891-20898.
- P. Prins, F. C. Grozema, J. M. Schins, S. Patil, U. Scherf and L. D. A. Siebbeles, *Phys. Rev. Lett.*, 2006, **96**, 146601.
- J. Sukegawa, C. Schubert, X. Zhu, H. Tsuji, D. M. Guldi and E. Nakamura, *Nat. Chem.*, 2014, **6**, 899-905.
- H. S. Cho, D. H. Jeong, S. Cho, D. Kim, Y. Matsuzaki, K. Tanaka, A. Tsuda and A. Osuka, *J. Am. Chem. Soc.*, 2002, **124**, 14642-14654.
- W. Zheng, T. Ikai and E. Yashima, *Angew. Chem. Int. Ed.*, 2021, **60**, 11294-11299.
- K. A. Mazzio and C. K. Luscombe, *Chem. Soc. Rev.*, 2015, **44**, 78-90.
- B. Geffroy, P. le Roy and C. Prat, *Polym. Int.*, 2006, **55**, 572-582.
- H. Siringhaus, *Adv. Mater.*, 2014, **26**, 1319-1335.
- Y. C. Teo, H. W. H. Lai and Y. Xia, *Chem. Eur. J.*, 2017, **23**, 14101-14112.
- R. L. Van Deusen, *J. Polym. Sci. Part B: Polym. Lett.*, 1966, **4**, 211-214.
- A. D. Schlüter, M. Löffler and V. Enkelmann, *Nature*, 1994, **368**, 831-834.
- S. W. Thomas, T. M. Long, B. D. Pate, S. R. Kline, E. L. Thomas and T. M. Swager, *J. Am. Chem. Soc.*, 2005, **127**, 17976-17977.
- U. Scherf and K. Müllen, *Die Makromol. Chemie, Rapid Commun.*, 1991, **12**, 489-497.
- K. Chmil and U. Scherf, *Die Makromol. Chemie, Rapid Commun.*, 1993, **14**, 217-222.
- J. M. Tour and J. J. S. Lamba, *J. Am. Chem. Soc.*, 1993, **115**, 4935-4936.
- Z. Yuan, Y. Xiao, Y. Yang and T. Xiong, *Macromolecules*, 2011, **44**, 1788-1791.
- J. Lee, B. B. Rajeeva, T. Yuan, Z.-H. Guo, Y.-H. Lin, M. Al-Hashimi, Y. Zheng and L. Fang, *Chem. Sci.*, 2016, **7**, 881-889.
- A. Narita, X. L. Feng, Y. Hernandez, S. A. Jensen, M. Bonn, H. F. Yang, I. A. Verzhbitskiy, C. Casiraghi, M. R. Hansen, A. H. R. Koch, G. Fytas, O. Ivasenko, B. Li, K. S. Mali, T. Balandina, S. Mahesh, S. De Feyter and K. Müllen, *Nat. Chem.*, 2014, **6**, 126-132.
- S. R. Bheemireddy, M. P. Hautzinger, T. Li, B. Lee and K. N. Plunkett, *J. Am. Chem. Soc.*, 2017, **139**, 5801-5807.
- A. V. Talyzin, I. V. Anoshkin, A. V. Krasheninnikov, R. M. Nieminen, A. G. Nasibulin, H. Jiang and E. I. Kauppinen, *Nano Lett.*, 2011, **11**, 4352-4356.
- T. Kitao, M. W. A. MacLean, K. Nakata, M. Takayanagi, M. Nagaoka and T. Uemura, *J. Am. Chem. Soc.*, 2020, **142**, 5509-5514.



30. X. Zhang, T. Kitao, D. Piga, R. Hongu, S. Bracco, A. Comotti, P. Sozzani and T. Uemura, *Chem. Sci.*, 2020, **11**, 10844-10849.
31. C.-G. Wu and T. Bein, *Science*, 1994, **266**, 1013-1015.
32. P. A. Held, H. Fuchs and A. Studer, *Chem. Eur. J.*, 2017, **23**, 5874-5892.
33. L. Grill and S. Hecht, *Nat. Chem.*, 2020, **12**, 115-130.
34. S.-W. Hla, L. Bartels, G. Meyer and K.-H. Rieder, *Phys. Rev. Lett.*, 2000, **85**, 2777-2780.
35. L. Grill, M. Dyer, L. Lafferentz, M. Persson, M. V. Peters and S. Hecht, *Nat. Nanotechnol.*, 2007, **2**, 687-691.
36. N. Lin, S. Stepanow, M. Ruben and J. V. Barth, *Top. Curr. Chem.*, 2009, **287**, 1-44.
37. H. Sakaguchi, H. Matsumura and H. Gong, *Nat. Mater.*, 2004, **3**, 551-557.
38. O. Ourdjini, R. Pawlak, M. Abel, S. Clair, L. Chen, N. Bergeon, M. Sassi, V. Oison, J.-M. Debierre, R. Coratger and L. Porte, *Phys. Rev. B*, 2011, **84**, 125421.
39. M. Bieri, M.-T. Nguyen, O. Gröning, J. Cai, M. Treier, K. Ait-Mansour, P. Ruffieux, C. A. Pignedoli, D. Passerone, M. Kastler, K. Müllen and R. Fasel, *J. Am. Chem. Soc.*, 2010, **132**, 16669-16676.
40. T. Miura, T. Kitao and T. Uemura, *J. Phys. Chem. C*, 2022, **126**, 6628-6636.
41. T. Kitao, S. Bracco, A. Comotti, P. Sozzani, M. Naito, S. Seki, T. Uemura and S. Kitagawa, *J. Am. Chem. Soc.*, 2015, **137**, 5231-5238.
42. F. Cucinotta, F. Carniato, G. Paul, S. Bracco, C. Bisio, S. Caldarelli and L. Marchese, *Chem. Mater.*, 2011, **23**, 2803-2809.
43. A. N. Khlobystov, D. A. Britz and G. A. D. Briggs, *Acc. Chem. Res.*, 2005, **38**, 901-909.
44. M. Nagata, S. Shukla, Y. Nakanishi, Z. Liu, Y.-C. Lin, T. Shiga, Y. Nakamura, T. Koyama, H. Kishida, T. Inoue, N. Kanda, S. Ohno, Y. Sakagawa, K. Suenaga and H. Shinohara, *Nano Lett.*, 2019, **19**, 4845-4851.
45. A. Botos, J. Biskupek, T. W. Chamberlain, G. A. Rance, C. T. Stoppello, J. Sloan, Z. Liu, K. Suenaga, U. Kaiser and A. N. Khlobystov, *J. Am. Chem. Soc.*, 2016, **138**, 8175-8183.
46. S. A. Miners, G. A. Rance and A. N. Khlobystov, *Chem. Soc. Rev.*, 2016, **45**, 4727-4746.
47. J. Zhang, Z. Zhu, Y. Feng, H. Ishiwata, Y. Miyata, R. Kitaura, J. E. P. Dahl, R. M. K. Carlson, N. A. Fokina, P. R. Schreiner, D. Tománek and H. Shinohara, *Angew. Chem. Int. Ed.*, 2013, **52**, 3717-3721.
48. T. Pichler, H. Kuzmany, H. Kataura and Y. Achiba, *Phys. Rev. Lett.*, 2001, **87**, 267401.
49. A. Comotti, S. Bracco, M. Mauri, S. Mottadelli, T. Ben, S. Qiu and P. Sozzani, *Angew. Chem. Int. Ed.*, 2012, **51**, 10136-10140.
50. A. Comotti, S. Bracco, M. Beretta, J. Perego, M. Gemmi and P. Sozzani, *Chem. Eur. J.*, 2015, **21**, 18209-18217.
51. T. Kitao, Y. Zhang, S. Kitagawa, B. Wang and T. Uemura, *Chem. Soc. Rev.*, 2017, **46**, 3108-3133.
52. M. Miyata, K. Morioka and K. Takemoto, *J. Polym. Sci., Polym. Chem. Ed.*, 1977, **15**, 2987-2996.
53. M. Miyata, Y. Kitahara, Y. Osaki and K. Takemoto, *J. Incl. Phenom.*, 1984, **2**, 391-398.
54. D. Zhao, J. Feng, Q. Huo, N. Melosh, G. H. Fredrickson, B. F. Chmelka and G. D. Stucky, *Science*, 1998, **279**, 548-552.
55. S. M. Ng, S.-i. Ogino, T. Aida, K. A. Koyano and T. Tatsumi, *Macromol. Rapid Commun.*, 1997, **18**, 991-996.
56. T.-Q. Nguyen, J. Wu, V. Doan, B. J. Schwartz and S. H. Tolbert, *Science*, 2000, **288**, 652-656.
57. A. J. Cadby and S. H. Tolbert, *J. Phys. Chem. B*, 2005, **109**, 17879-17886.
58. S. Kitagawa, R. Kitaura and S. Noro, *Angew. Chem. Int. Ed.*, 2004, **43**, 2334-2375.
59. H. Furukawa, K. E. Cordova, M. O'Keeffe and O. M. Yaghi, *Science*, 2013, **341**, 1230444.
60. G. Férey, *Chem. Soc. Rev.*, 2008, **37**, 191-214.
61. K. Sumida, D. L. Rogow, J. A. Mason, T. M. McDonald, E. D. Bloch, Z. R. Herm, T.-H. Bae and J. R. Long, *Chem. Rev.*, 2012, **112**, 724-781.
62. P. Horcajada, T. Chalati, C. Serre, B. Gillet, C. Sebrie, T. Baati, J. F. Eubank, D. Heurtaux, P. Clayette and C. Kreuz, *Nat. Mater.*, 2010, **9**, 172-178.
63. L. E. Kreno, K. Leong, O. K. Farha, M. Allendorf, R. P. Van Duyne and J. T. Hupp, *Chem. Rev.*, 2011, **112**, 1105-1125.
64. J.-R. Li, R. J. Kuppler and H.-C. Zhou, *Chem. Soc. Rev.*, 2009, **38**, 1477-1504.
65. N. Hosono and T. Uemura, *Acc. Chem. Res.*, 2021, **54**, 3593-3603.
66. T. Uemura, K. Kitagawa, S. Horike, T. Kawamura, S. Kitagawa, M. Mizuno and K. Endo, *Chem. Commun.*, 2005, 5968-5970.
67. B. V. K. J. Schmidt, *Macromol. Rapid Commun.*, 2020, **41**, 1900333.
68. M. S. Denny Jr, J. C. Moreton, L. Benz and S. M. Cohen, *Nat. Rev. Mater.*, 2016, **1**, 16078.
69. S. Begum, Z. Hassan, S. Bräse and M. Tsotsalas, *Langmuir*, 2020, **36**, 10657-10673.
70. N. Ding, H. Li, X. Feng, Q. Wang, S. Wang, L. Ma, J. Zhou and B. Wang, *J. Am. Chem. Soc.*, 2016, **138**, 10100-10103.
71. M. W. MacLean, T. Kitao, T. Suga, M. Mizuno, S. Seki, T. Uemura and S. Kitagawa, *Angewandte Chemie International Edition*, 2016, **55**, 708-713.
72. B. Le Ouay, M. Boudot, T. Kitao, T. Yanagida, S. Kitagawa and T. Uemura, *J. Am. Chem. Soc.*, 2016, **138**, 10088-10091.
73. C. Lu, T. Ben, S. Xu and S. Qiu, *Angew. Chem. Int. Ed.*, 2014, **53**, 6454-6458.
74. Y. Kobayashi, Y. Horie, K. Honjo, T. Uemura and S. Kitagawa, *Chem. Commun.*, 2016, **52**, 5156-5159.
75. Y. Kobayashi, K. Honjo, S. Kitagawa and T. Uemura, *ACS Appl. Mater. Interfaces*, 2017, **9**, 11373-11379.
76. H.-C. Lee, J. Hwang, U. Schilde, M. Antonietti, K. Matyjaszewski and B. V. K. J. Schmidt, *Chem. Mater.*, 2018, **30**, 2983-2994.
77. T. Uemura, Y. Ono, K. Kitagawa and S. Kitagawa, *Macromolecules*, 2008, **41**, 87-94.
78. T. Uemura, N. Uchida, M. Higuchi and S. Kitagawa, *Macromolecules*, 2011, **44**, 2693-2697.
79. G. Distefano, H. Suzuki, M. Tsujimoto, S. Isoda, S. Bracco, A. Comotti, P. Sozzani, T. Uemura and S. Kitagawa, *Nat. Chem.*, 2013, **5**, 335-341.
80. T. Kitao, M. W. MacLean, B. Le Ouay, Y. Sasaki, M. Tsujimoto, S. Kitagawa and T. Uemura, *Polym. Chem.*, 2017, **8**, 5077-5081.
81. T. Uemura, Y. Ono and S. Kitagawa, *Chem. Lett.*, 2008, **37**, 616-617.
82. S. Mochizuki, N. Ogiwara, M. Takayanagi, M. Nagaoka, S. Kitagawa and T. Uemura, *Nat. Commun.*, 2018, **9**, 329.

83. T. Kitao, Y. Nagasaka, M. Karasawa, T. Eguchi, N. Kimizuka, K. Ishii, T. Yamada and T. Uemura, *J. Am. Chem. Soc.*, 2019, **141**, 19565-19569.
84. N. Hosono, S. Mochizuki, Y. Hayashi and T. Uemura, *Nat. Commun.*, 2020, **11**, 3573.
85. N. Yanai, T. Uemura, M. Ohba, Y. Kadowaki, M. Maesato, M. Takenaka, S. Nishitsuji, H. Hasegawa and S. Kitagawa, *Angew. Chem. Int. Ed.*, 2008, **47**, 9883-9886.
86. T. Uemura, Y. Kadowaki, N. Yanai and S. Kitagawa, *Chem. Mater.*, 2009, **21**, 4096-4098.
87. M. Tsotsalas, J. Liu, B. Tettmann, S. Grosjean, A. Shahnas, Z. Wang, C. Azucena, M. Addicoat, T. Heine, J. Lahann, J. Overhage, S. Bräse, H. Gliemann and C. Wöll, *J. Am. Chem. Soc.*, 2014, **136**, 8-11.
88. T. Ishiwata, Y. Furukawa, K. Sugikawa, K. Kokado and K. Sada, *J. Am. Chem. Soc.*, 2013, **135**, 5427-5432.
89. T. Uemura, D. Hiramatsu, Y. Kubota, M. Takata and S. Kitagawa, *Angew. Chem.*, 2007, **119**, 5075-5078.
90. T. Uemura, R. Nakanishi, T. Kaseda, N. Uchida and S. Kitagawa, *Macromolecules*, 2014, **47**, 7321-7326.
91. Y. W. Son, M. L. Cohen and S. G. Louie, *Phys. Rev. Lett.*, 2006, **97**, 4.
92. S. Dutta and S. K. Pati, *J. Mater. Chem.*, 2010, **20**, 8207-8223.
93. M. Terrones, A. R. Botello-Mendez, J. Campos-Delgado, F. Lopez-Urias, Y. I. Vega-Cantu, F. J. Rodriguez-Macias, A. L. Elias, E. Munoz-Sandoval, A. G. Cano-Marquez, J. C. Charlier and H. Terrones, *Nano Today*, 2010, **5**, 351-372.
94. K. Nakada, M. Fujita, G. Dresselhaus and M. S. Dresselhaus, *Phys. Rev. B*, 1996, **54**, 17954-17961.
95. M. Y. Han, B. Ozyilmaz, Y. B. Zhang and P. Kim, *Phys. Rev. Lett.*, 2007, **98**, 4.
96. D. J. Rizzo, G. Veber, J. Jiang, R. McCurdy, T. Cao, C. Bronner, T. Chen, S. G. Louie, F. R. Fischer and M. F. Crommie, *Science*, 2020, **369**, 1597-1603.
97. D. V. Kosynkin, A. L. Higginbotham, A. Sinitskii, J. R. Lomeda, A. Dimiev, B. K. Price and J. M. Tour, *Nature*, 2009, **458**, 872-U875.
98. X. Wang and H. Dai, *Nature Chem.*, 2010, **2**, 661.
99. C. Chen, Y. Lin, W. Zhou, M. Gong, Z. He, F. Shi, X. Li, J. Z. Wu, K. T. Lam, J. N. Wang, F. Yang, Q. Zeng, J. Guo, W. Gao, J.-M. Zuo, J. Liu, G. Hong, A. L. Antaris, M.-C. Lin, W. L. Mao and H. Dai, *Nat. Electron.*, 2021, **4**, 653-663.
100. J. M. Cai, P. Ruffieux, R. Jaafar, M. Bierl, T. Braun, S. Blankenburg, M. Muoth, A. P. Seitsonen, M. Saleh, X. L. Feng, K. Müllen and R. Fasel, *Nature*, 2010, **466**, 470-473.
101. J. Björk, S. Stafström and F. Hanke, *J. Am. Chem. Soc.*, 2011, **133**, 14884-14887.
102. H. Sakaguchi, Y. Kawagoe, Y. Hirano, T. Iruka, M. Yano and T. Nakae, *Adv. Mater.*, 2014, **26**, 4134-4138.
103. Z. Liu, H. Qiu, C. Wang, Z. Chen, B. Zyska, A. Narita, A. Ciesielski, S. Hecht, L. Chi, K. Müllen and P. Samorì, *Adv. Mater.*, 2020, **32**, 2001268.
104. G. Li, K.-Y. Yoon, X. Zhong, J. Wang, R. Zhang, J. R. Guest, J. Wen, X. Y. Zhu and G. Dong, *Nat. Commun.*, 2018, **9**, 1687.
105. J. P. Llinas, A. Fairbrother, G. Borin Barin, W. Shi, K. Lee, S. Wu, B. Yong Choi, R. Braganza, J. Lear, N. Kau, W. Choi, C. Chen, Z. Pedramrazi, T. Dumsloff, A. Narita, X. Feng, K. Müllen, F. Fischer, A. Zettl, P. Ruffieux, E. Yablonovitch, M. Crommie, R. Fasel and J. Bokor, *Nat. Commun.*, 2017, **8**, 633.
106. J. Yamaguchi, H. Hayashi, H. Jippo, A. Shiotari, M. Ohtomo, M. Sakakura, N. Hieda, N. Aratani, M. Ohfuchi, Y. Sugimoto, H. Yamada and S. Sato, *Commun. Mater.*, 2020, **1**, 36.
107. A. Kimouche, M. M. Ervasti, R. Drost, S. Halonen, A. Harju, P. M. Joensuu, J. Sainio and P. Liljeroth, *Nat. Commun.*, 2015, **6**, 6.
108. Y.-C. Chen, D. G. de Oteyza, Z. Pedramrazi, C. Chen, F. R. Fischer and M. F. Crommie, *ACS Nano*, 2013, **7**, 6123-6128.
109. P. Han, K. Akagi, F. Federici Canova, H. Mutoh, S. Shiraki, K. Iwaya, P. S. Weiss, N. Asao and T. Hitosugi, *ACS Nano*, 2014, **8**, 9181-9187.
110. X.-Y. Wang, J. I. Urgel, G. B. Barin, K. Eimre, M. Di Giovannantonio, A. Milani, M. Tommasini, C. A. Pignedoli, P. Ruffieux, X. Feng, R. Fasel, K. Müllen and A. Narita, *J. Am. Chem. Soc.*, 2018, **140**, 9104-9107.
111. J. Li, S. Sanz, N. Merino-Díez, M. Vilas-Varela, A. Garcia-Lekue, M. Corso, D. G. de Oteyza, T. Frederiksen, D. Peña and J. I. Pascual, *Nat. Commun.*, 2021, **12**, 5538.
112. Q. Sun, O. Gröning, J. Overbeck, O. Braun, M. L. Perrin, G. Borin Barin, M. El Abbassi, K. Eimre, E. Ditle, C. Daniels, V. Meunier, C. A. Pignedoli, M. Calame, R. Fasel and P. Ruffieux, *Adv. Mater.*, 2020, **32**, 1906054.
113. C. Bronner, S. Stremmlau, M. Gille, F. Brauße, A. Haase, S. Hecht and P. Tegeder, *Angew. Chem. Int. Ed.*, 2013, **52**, 4422-4425.
114. K. Kawai, S. Saito, S. Osumi, S. Yamaguchi, A. S. Foster, P. Spijker and E. Meyer, *Nat. Commun.*, 2015, **6**, 8098.
115. R. R. Cloke, T. Marangoni, G. D. Nguyen, T. Joshi, D. J. Rizzo, C. Bronner, T. Cao, S. G. Louie, M. F. Crommie and F. R. Fischer, *J. Am. Chem. Soc.*, 2015, **137**, 8872-8875.
116. J. Cai, C. A. Pignedoli, L. Talirz, P. Ruffieux, H. Söde, L. Liang, V. Meunier, R. Berger, R. Li, X. Feng, K. Müllen and R. Fasel, *Nat. Nanotechnol.*, 2014, **9**, 896-900.
117. O. Gröning, S. Wang, X. Yao, C. A. Pignedoli, G. Borin Barin, C. Daniels, A. Cupo, V. Meunier, X. Feng, A. Narita, K. Müllen, P. Ruffieux and R. Fasel, *Nature*, 2018, **560**, 209-213.
118. J.-P. Joost, A.-P. Jauho and M. Bonitz, *Nano Lett.*, 2019, **19**, 9045-9050.
119. D. J. Rizzo, G. Veber, T. Cao, C. Bronner, T. Chen, F. Zhao, H. Rodriguez, S. G. Louie, M. F. Crommie and F. R. Fischer, *Nature*, 2018, **560**, 204-208.
120. C. Bronner, R. A. Durr, D. J. Rizzo, Y.-L. Lee, T. Marangoni, A. M. Kalayjian, H. Rodriguez, W. Zhao, S. G. Louie, F. R. Fischer and M. F. Crommie, *ACS Nano*, 2018, **12**, 2193-2200.
121. P. Ruffieux, S. Wang, B. Yang, C. Sánchez-Sánchez, J. Liu, T. Dienel, L. Talirz, P. Shinde, C. A. Pignedoli, D. Passerone, T. Dumsloff, X. Feng, K. Müllen and R. Fasel, *Nature*, 2016, **531**, 489-492.
122. R. E. Blackwell, F. Zhao, E. Brooks, J. Zhu, I. Piskun, S. Wang, A. Delgado, Y.-L. Lee, S. G. Louie and F. R. Fischer, *Nature*, 2021, **600**, 647-652.
123. A. Batra, D. Cvetko, G. Kladnik, O. Adak, C. Cardoso, A. Ferretti, D. Prezzi, E. Molinari, A. Morgante and L. Venkataraman, *Chem. Sci.*, 2014, **5**, 4419-4423.
124. L. Talirz, H. Söde, J. Cai, P. Ruffieux, S. Blankenburg, R. Jafaar, R. Berger, X. Feng, K. Müllen, D. Passerone, R. Fasel and C. A. Pignedoli, *J. Am. Chem. Soc.*, 2013, **135**, 2060-2063.
125. M. Di Giovannantonio, O. Deniz, J. I. Urgel, R. Widmer, T. Dienel, S. Stolz, C. Sánchez-Sánchez, M. Muntwiler, T.

- Dumslaff, R. Berger, A. Narita, X. Feng, K. Müllen, P. Ruffieux and R. Fasel, *ACS Nano*, 2018, **12**, 74-81.
126. A. Basagni, F. Sedona, C. A. Pignedoli, M. Cattelan, L. Nicolas, M. Casarin and M. Sambri, *J. Am. Chem. Soc.*, 2015, **137**, 1802-1808.
127. C. Moreno, M. Paradinas, M. Vilas-Varela, M. Panighel, G. Ceballos, D. Peña and A. Mugarza, *Chem. Commun.*, 2018, **54**, 9402-9405.
128. L. Grossmann, B. T. King, S. Reichlmaier, N. Hartmann, J. Rosen, W. M. Heckl, J. Björk and M. Lackinger, *Nature Chem.*, 2021, **13**, 730-736.
129. C. Moreno, M. Vilas-Varela, B. Kretz, A. Garcia-Lekue, M. V. Costache, M. Paradinas, M. Panighel, G. Ceballos, S. O. Valenzuela, D. Peña and A. Mugarza, *Science*, 2018, **360**, 199-203.
130. M. Koudia and M. Abel, *Chem. Commun.*, 2014, **50**, 8565-8567.
131. P. H. Jacobse, R. D. McCurdy, J. Jiang, D. J. Rizzo, G. Veber, P. Butler, R. Zuzak, S. G. Louie, F. R. Fischer and M. F. Crommie, *J. Am. Chem. Soc.*, 2020, **142**, 13507-13514.
132. Z. Mutlu, P. H. Jacobse, R. D. McCurdy, J. P. Llinas, Y. Lin, G. C. Veber, F. R. Fischer, M. F. Crommie and J. Bokor, *Adv. Funct. Mater.*, 2021, **31**, 2103798.
133. A. Chuvilin, E. Bichoutskaia, M. C. Gimenez-Lopez, T. W. Chamberlain, G. A. Rance, N. Kuganathan, J. Biskupek, U. Kaiser and A. N. Khlobystov, *Nat. Mater.*, 2011, **10**, 687-692.
134. T. W. Chamberlain, J. Biskupek, G. A. Rance, A. Chuvilin, T. J. Alexander, E. Bichoutskaia, U. Kaiser and A. N. Khlobystov, *ACS Nano*, 2012, **6**, 3943-3953.
135. H. E. Lim, Y. Miyata, R. Kitaura, Y. Nishimura, Y. Nishimoto, S. Irle, J. H. Warner, H. Kataura and H. Shinohara, *Nat. Commun*, 2013, **4**, 2548.
136. H. E. Lim, Y. Miyata, M. Fujihara, S. Okada, Z. Liu, Arifin, K. Sato, H. Omachi, R. Kitaura, S. Irle, K. Suenaga and H. Shinohara, *ACS Nano*, 2015, **9**, 5034-5040.
137. I. V. Lebedeva, A. M. Popov, A. A. Knizhnik, A. N. Khlobystov and B. V. Potapkin, *Nanoscale*, 2012, **4**, 4522-4529.
138. R. Thakur, P. K. Ahluwalia, A. Kumar, M. Sharma and R. Sharma, *Euro. Phys. J. B*, 2021, **94**, 99.
139. X.-Y. Xie, J.-J. Yang, X.-Y. Liu, Q. Fang, W.-H. Fang and G. Cui, *Phys. Chem. Chem. Phys.*, 2021, **23**, 13503-13511.
140. V. Guillermin, F. Ragon, M. Dan-Hardi, T. Devic, M. Vishnuvarthan, B. Campo, A. Vimont, G. Clet, Q. Yang, G. Maurin, G. Ferey, A. Vittadini, S. Gross and C. Serre, *Angew. Chem. Int. Ed.*, 2012, **51**, 9267-9271.
141. G. Tamaki, T. Kawakami and M. Koshino, *Phys. Rev. B*, 2020, **101**, 205311.
142. Y. Tobe, *Top. Curr. Chem.*, 2018, **376**, 12.
143. P. Hu, S. Lee, T. S. Heng, N. Aratani, T. P. Gonçalves, Q. Qi, X. Shi, H. Yamada, K.-W. Huang, J. Ding, D. Kim and J. Wu, *J. Am. Chem. Soc.*, 2016, **138**, 1065-1077.
144. C. K. Frederickson, B. D. Rose and M. M. Haley, *Acc. Chem. Res.*, 2017, **50**, 977-987.
145. J. M. Schulman and R. L. Disch, *J. Am. Chem. Soc.*, 1996, **118**, 8470-8474.
146. T. A. Albright, P. I. Dosa, T. N. Grossmann, V. N. Khrustalev, O. A. Oloba, R. Padilla, R. Paubelle, A. Stanger, T. V. Timofeeva and K. P. C. Vollhardt, *Angew. Chem. Int. Edit.*, 2009, **48**, 9853-9857.
147. D.-Y. Li, X. Qiu, S.-W. Li, Y.-T. Ren, Y.-C. Zhu, C.-H. Shu, X.-Y. Hou, M. Liu, X.-Q. Shi, X. Qiu and P.-N. Liu, *J. Am. Chem. Soc.*, 2021, **143**, 12955-12960.
148. P. H. Jacobse, Z. Jin, J. Jiang, S. Peurifoy, Z. Yue, Z. Wang, D. J. Rizzo, S. G. Louie, C. Nuckolls and M. F. Crommie, *Sci. Adv.*, 2021, **7**, eabl5892.
149. C. Sánchez-Sánchez, T. Dienel, A. Nicolaï, N. Khariche, L. Liang, C. Daniels, V. Meunier, J. Liu, X. Feng, K. Müllen, J. R. Sánchez-Valencia, O. Gröning, P. Ruffieux and R. Fasel, *Chem. Eur. J.*, 2019, **25**, 12074-12082.
150. U. Scherf and K. Müllen, *Polymer*, 1992, **33**, 2443-2446.
151. M. Di Giovannantonio, Q. Chen, J. I. Urgel, P. Ruffieux, C. A. Pignedoli, K. Müllen, A. Narita and R. Fasel, *J. Am. Chem. Soc.*, 2020, **142**, 12925-12929.
152. B. de la Torre, A. Matěj, A. Sánchez-Grande, B. Cirera, B. Mallada, E. Rodríguez-Sánchez, J. Santos, J. I. Mendieta-Moreno, S. Edalatmanesh, K. Lauwaet, M. Otyepka, M. Medved', Á. Buendía, R. Miranda, N. Martín, P. Jelínek and D. Écija, *Nat. Commun.*, 2020, **11**, 4567.
153. C. Glidewell and D. Lloyd, *Tetrahedron*, 1984, **40**, 4455-4472.
154. O. El Bakouri, J. Poater, F. Feixas and M. Solà, *Theor. Chem. Acc.*, 2016, **135**, 205.
155. Q. Fan, D. Martin-Jimenez, D. Ebeling, C. K. Krug, L. Brechmann, C. Kohlmeyer, G. Hilt, W. Hieringer, A. Schirmeisen and J. M. Gottfried, *J. Am. Chem. Soc.*, 2019, **141**, 17713-17720.
156. M. Liu, M. Liu, L. She, Z. Zha, J. Pan, S. Li, T. Li, Y. He, Z. Cai, J. Wang, Y. Zheng, X. Qiu and D. Zhong, *Nat. Commun.*, 2017, **8**, 14924.
157. A. Tsuda and A. Osuka, *Science*, 2001, **293**, 79-82.
158. A. Wiengarten, K. Seufert, W. Auwärter, D. Ecija, K. Diller, F. Allegretti, F. Bischoff, S. Fischer, D. A. Duncan, A. C. Papageorgiou, F. Klappenberger, R. G. Acres, T. H. Ngo and J. V. Barth, *J. Am. Chem. Soc.*, 2014, **136**, 9346-9354.
159. Q. Sun, L. M. Mateo, R. Robles, N. Lorente, P. Ruffieux, G. Bottari, T. Torres and R. Fasel, *Angew. Chem. Int. Ed.*, 2021, **60**, 16208-16214.
160. S. Chand, *J. Mater. Sci.*, 2000, **35**, 1303-1313.
161. M. S. A. Rahaman, A. F. Ismail and A. Mustafa, *Polym. Degrad. Stab.*, 2007, **92**, 1421-1432.
162. B. L. Huang, A. J. H. McGaughey and M. Kaviani, *Int. J. Heat Mass Transf.*, 2007, **50**, 393-404.
163. T. Uemura, N. Yanai, S. Watanabe, H. Tanaka, R. Numaguchi, M. T. Miyahara, Y. Ohta, M. Nagaoka and S. Kitagawa, *Nat. Commun.*, 2010, **1**, 83.
164. N. Oe, N. Hosono and T. Uemura, *Chem. Sci.*, 2021, **12**, 12576-12586.
165. N. Mizutani, N. Hosono, B. Le Ouay, T. Kitao, R. Matsuura, T. Kubo and T. Uemura, *J. Am. Chem. Soc.*, 2020, **142**, 3701-3705.
166. Y. Zou, X. Ji, J. Cai, T. Yuan, D. J. Stanton, Y.-H. Lin, M. Naraghi and L. Fang, *Chem*, 2017, **2**, 139-152.
167. S. Lone, A. Bhardwaj, A. K. Pandit, S. Gupta and S. Mahajan, *J. Electron. Mater.*, 2021, **50**, 3169-3186.
168. Q. Sun, C. Zhang, Z. Li, H. Kong, Q. Tan, A. Hu and W. Xu, *J. Am. Chem. Soc.*, 2013, **135**, 8448-8451.
169. M. Kolmer, A.-K. Steiner, I. Izydorczyk, W. Ko, M. Engelund, M. Szymonski, A.-P. Li and K. Amsharov, *Science*, 2020, **369**, 571-575.

170. K. Kimura, K. Miwa, H. Imada, M. Imai-Imada, S. Kawahara, J. Takeya, M. Kawai, M. Galperin and Y. Kim, *Nature*, 2019, **570**, 210-213.
171. H. Dai, *Acc. Chem. Res.*, 2002, **35**, 1035-1044.
172. H. Omachi, Y. Segawa and K. Itami, *Acc. Chem. Res.*, 2012, **45**, 1378-1389.
173. S. Wang, T. Kitao, N. Guillou, M. Wahiduzzaman, C. Martineau-Corcus, F. Nouar, A. Tissot, L. Binet, N. Ramsahye, S. Devautour-Vinot, S. Kitagawa, S. Seki, Y. Tsutsui, V. Briois, N. Steunou, G. Maurin, T. Uemura and C. Serre, *Nat. Commun.*, 2018, **9**, 1660.
174. S.-W. Lo, T. Kitao, Y. Nada, K. Murata, K. Ishii and T. Uemura, *Angew. Chem. Int. Ed.*, 2021, **60**, 17947-17951.
175. M. Zeng, A. Ren, W. Wu, Y. Zhao, C. Zhan and J. Yao, *Chem. Scie.*, 2020, **11**, 9154-9161.